

See discussions, stats, and author profiles for this publication at: <https://www.researchgate.net/publication/262381382>

# Controllable Growth of CNTs on Graphene as High-Performance Electrode Material for Supercapacitor.

ARTICLE in ACS APPLIED MATERIALS & INTERFACES · MAY 2014

Impact Factor: 6.72 · DOI: 10.1021/am501362g · Source: PubMed

---

CITATIONS

14

READS

37

## 7 AUTHORS, INCLUDING:



[Lin Jing](#)

University of New South Wales

14 PUBLICATIONS 111 CITATIONS

[SEE PROFILE](#)



[Yiming Yan](#)

Beijing Institute of Technology

50 PUBLICATIONS 1,997 CITATIONS

[SEE PROFILE](#)



[Kening Sun](#)

Harbin Institute of Technology

146 PUBLICATIONS 1,448 CITATIONS

[SEE PROFILE](#)

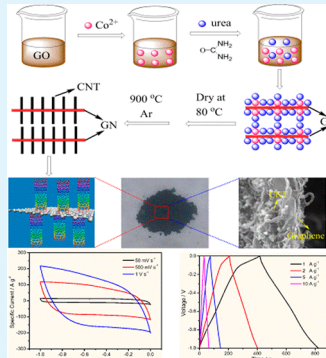
# Controllable Growth of CNTs on Graphene as High-Performance Electrode Material for Supercapacitors

Zhi-Yu Yang, Yu-Fei Zhao, Qing-Qing Xiao, Yu-Xia Zhang, Lin Jing, Yi-Ming Yan,\* and Ke-Ning Sun\*

Beijing Key Laboratory for Chemical Power Source and Green Catalysis, School of Chemical Engineering and Environment, Beijing Institute of Technology, Beijing, 100081, People's Republic of China

## S Supporting Information

**ABSTRACT:** Design and synthesis of three-dimensional (3D) structured carbon materials are crucial for achieving high-performance supercapacitors (SC) for energy storage. Here, we report the preparation of 3D architectured GN-CNT hybrid as SC electrodes. Controllable growth of carbon nanotubes on graphene sheets was realized through a facile one-pot pyrolysis strategy. The length of the carbon nanotubes could be rationally tuned by adjusting the amount of precursors. Correspondingly, the resulted GN-CNT hybrid showed adjustable electrochemical performance as an SC electrode. Importantly, the GN-CNT exhibited a high specific surface area of  $903 \text{ m}^2 \text{ g}^{-1}$  and maximum specific capacitance of  $413 \text{ F g}^{-1}$  as SC electrodes at a scan rate of  $5 \text{ mV s}^{-1}$  in  $6 \text{ M KOH}$  aqueous solution. This work paves a feasible pathway to prepare carbon electrode materials with favorable 3D architecture and high performance, for use in energy storage and conversion.



**KEYWORDS:** one-pot strategy, controllable growth, graphene, carbon nanotube, 3D architecture, supercapacitor

## INTRODUCTION

Carbon-based materials, such as activated carbons, carbon nanotubes (CNTs), graphene, and their derivatives, have received tremendous attention for their superior thermal, electrical, and mechanical properties suitable for a wide range of applications.<sup>1–5</sup> In particular, new systems of carbon materials with unique architectures have been emerged as appealing candidates for their pronounced properties and boosting performance, especially toward the applications of energy storage and conversion.<sup>6–11</sup> Among the members of carbon family, CNTs represent classic one-dimensional (1D) structured carbon materials, possessing distinct mechanical properties, large theoretical surface area, good electronic conductivity, and high electrochemical stability. Meanwhile, graphene, consisting of a single layer or a few layers of graphitic carbon, is a typical two-dimensional (2D) structural material, which has been demonstrated as an ideal scaffold for doping elements or functionalizing components. In recent years, a series of studies on combining 1D CNTs with 2D graphene nanosheets (GN), with the assumption of forming a unique 3D architecture of carbon materials, have been reported for a variety of applications.<sup>12–14</sup> Apart from taking the advantage of the formed open and porous network in the resultant hybrid, these efforts are believed to largely exploit the properties and improve the performance of the fabricated devices based on a possible synergistic effect between two different graphitic components. For example, theoretical simulations have assuredly predicted that a 3D nanocomposite, building with layered graphene spaced by vertically aligned carbon nanotubes, could exhibit

fascinating out-of-plane transport and mechanical properties, maintaining the remarkable character of such architectures.<sup>15,16</sup>

To obtain such 3D architectures of GN-CNT hybrids experimentally, some strategies have been successfully developed. For instance, CNTs grown on graphene film were obtained by spin-coating graphene oxide on  $\text{SiO}_2/\text{Si}$  wafer, deposition of iron, and plasma-enhanced chemical vapor deposition (PECVD).<sup>6</sup> 3D pillared VACNT-graphene architecture was also prepared by thermal expansion of highly ordered pyrolytic graphite, followed by a high-temperature  $\text{SiO}_2$  coating and the growth of CNTs by means of pyrolysis of FePc.<sup>17</sup> Also, a CNT–graphene sandwich (CGS) was synthesized through microwave treatment and a subsequent chemical vapor deposition (CVD) method.<sup>18</sup> In addition, electrostatic spray deposition and photolithography liftoff was reported to fabricate reduced graphene oxide composites through combination with CNTs.<sup>19</sup> In addition, layer-by-layer (LbL) self-assembly and liquid-phase reaction have also been explored to fabricate the GN-CNT hybrids.<sup>20</sup> However, these reported methods were found to be limited in their practical applications, either because of their uncontrollable and complicated manipulations, or because of the unsatisfied performance of the resultant materials. Therefore, it is desirable to search for a novel strategy to fabricate typical 3D porous structural GN-CNT hybrid with high performance.

**Received:** March 7, 2014

**Accepted:** May 15, 2014

**Published:** May 15, 2014

On the other hand, GN-CNT hybrid is an attractive electrode material of supercapacitors (SCs) for energy-storage applications. Although it is known that graphene possess a maximum theoretical gravimetric specific double-layer capacitance of  $\sim 550 \text{ F g}^{-1}$ ,<sup>21</sup> the reported specific capacitances of graphene-based materials, such as 3D CGS or self-assembled graphene–CNT films, are far lower than the theoretical value. Such a gap is mainly ascribed to both the structural defects and the ineffective electrical properties of the prepared GN-CNT hybrid, which could be reasonably resolved by designing a route to fabricate rationally structured GN-CNT hybrid with high performance.

In this work, we report, for the first time, on a one-pot pyrolysis strategy to prepare 3D interpenetrating nanostructured GN-CNT hybrid. We demonstrate that controllable growth of CNT on GN could be easily realized with this novel method, in addition to obtain a well-defined 3D structural GN-CNT composite raised from the unique pyrolysis process. Importantly, the as-prepared GN-CNT not only possesses high specific surface area of  $903 \text{ m}^2 \text{ g}^{-1}$ , but also exhibits significant specific capacitance of  $413 \text{ F g}^{-1}$  as SC electrodes at a scan rate of  $5 \text{ mV s}^{-1}$  in 6 M KOH aqueous solution. The as-fabricated SC based on GN-CNT clearly outperforms the previously reported results obtained with other GN-CNT-, GN-, or CNT-based SCs, in terms of the specific capacitance and durability.

## EXPERIMENTAL SECTION

**Synthesis of the GN-CNT Hybrids and GN.** The graphite oxide (GO) was synthesized from natural graphite flake (Alfa Aesar, 325 mesh) by a modified Hummers method.<sup>22</sup> To synthesize GN-CNT, 200 mg of GO was dispersed in 200 mL of water. Then, 0.29 g  $\text{Co}(\text{NO}_3)_2 \cdot 6\text{H}_2\text{O}$  was added into the solution, followed by stirring for 4 h at room temperature. After that, 6.0 g urea was introduced into the above suspension and the mixed solution was stirred continuously at  $80^\circ\text{C}$  until a gray powder was obtained. The gray powder was then transferred to a tube furnace and annealed at  $900^\circ\text{C}$  for 1 h under an argon atmosphere to obtain  $\text{GN-CNT}_{6.00}$ . In addition,  $\text{GN-CNT}_{30.0}$ ,  $\text{GN-CNT}_{15.0}$ , and  $\text{GN-Co-urea}_{3.0}$  were prepared by adding an additional amount of urea (30.0, 15.0, and 3.0 g in the same process, respectively). As a comparison, GN was prepared with the same procedure without the addition of  $\text{Co}(\text{NO}_3)_2 \cdot 6\text{H}_2\text{O}$  and urea.  $\text{GN-CNT}_{\text{blend}}$  was prepared by physically blending GN and commercial CNT with a mass ratio of 9:1.

**Material Characterization.** The morphology was characterized by scanning electron microscopy (SEM) (QUANTA, Model FEG 250) and transmission electron microscopy (TEM) (FEI Tecnai, Model G2 T30). Brunauer–Emmett–Teller (BET) measurements using  $\text{N}_2$  absorption was performed on Autosorb-IQ2-MP-C system. The obtained products were characterized by X-ray diffraction (Rigaku Ultima IV, Cu  $\text{K}\alpha$  radiation, 40 kV, 40 mA). Raman spectroscopy was performed on a Renishaw RM 2000 system with a 633-nm laser. X-ray photoelectron spectroscopy (XPS) (Physical Electronics, Model 5400 ESCA) was used to quantitatively analyze the chemical compositions of GN-CNT.

**Electrochemical Measurements.** Electrochemical measurements were performed in three-electrode cell configuration on electrochemical analyzer (CHI Instruments, Model 660). Polytetrafluoroethylene (PTFE) (Sigma-Aldrich; 60 wt % dispersion in water) was added to the mixture of samples and carbon black (samples/carbon/PTFE = 80 (10 mg):15 (1.9 mg):5 (0.6 mg) by weight) as a binder. The mixture was mixed into a paste using a mortar and pestle, and the slurry was pressed onto a nickel form and dried at  $60^\circ\text{C}$  under vacuum for use as working electrodes. A graphite sheet with identical weight and size with a working electrode was used as counter electrodes and saturated calomel electrodes were used as reference electrodes. The electrolyte was a 6 M KOH solution saturation with

nitrogen. The specific capacitance of the electrode can be calculated according to the following equation:

$$C = \frac{1}{\omega v(V_c - V_a)} \int_{V_a}^{V_c} I(V) dV \quad (1)$$

where  $C$  is the specific capacitance ( $\text{F g}^{-1}$ ),  $\omega$  is the mass of electroactive materials in the electrodes (g),  $v$  is the potential scan rate ( $\text{mV s}^{-1}$ ),  $V_c$  and  $V_a$  are the integration limits of the voltammetric curve (V), and  $I(V)$  denotes the response current density ( $\text{A cm}^{-2}$ ).

The specific capacitance from galvanostatic CD tests was calculated according to

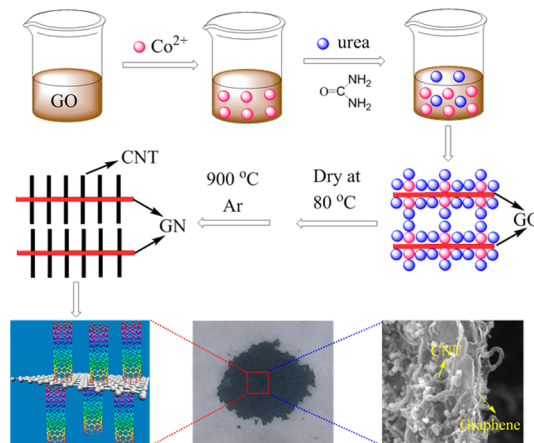
$$C = \left( \frac{I}{m} \right) \left( \frac{dV}{dt} \right) \quad (2)$$

where  $I$  is the applied current and  $m$  is the mass of electrode material; the term  $dV/dt$  is calculated from the slope of the discharge curves.

## RESULTS AND DISCUSSION

The strategy for the fabrication of GN-CNT hybrids is illustrated in Scheme 1. First, GO solution was prepared

**Scheme 1. Schematic Representation of the Procedure for the Preparation of the GN-CNT Hybrids**



through a general ultrasonic treatment. Then,  $\text{Co}^{2+}$  was introduced into the obtained solution with a thorough mixing process, which enables a full adsorption of  $\text{Co}^{2+}$  on the surface of GO via ion exchange between positively charged Co ions and the oxygen-containing functional groups. After that, a certain amount of urea was added into the mixture, and the hydrophilic urea could be easily inserted into the graphene layers and form complexes with  $\text{Co}^{2+}$ , resulting a stable mixture. Thus, it is assumed that the addition of urea may prevent the restack between GO sheets during the following drying and annealing process. On the other hand, urea can act as carbon resource during the annealing process for growing CNTs. Finally, we noted that the annealing process is a key step for the growth of CNTs on graphene sheet on the aid of the existence of cobalt species. It was reported that the pyrolysis of urea may produce carbon nitride, accompanied by the release of gas.<sup>23</sup> As a consequence, in our case, a large amount of carbon nitride gases (e.g.,  $\text{C}_2\text{N}_2^+$ ,  $\text{C}_3\text{N}_2^+$ ,  $\text{C}_3\text{N}_3^+$ ) could be produced with the elevation of temperature, which is believed to loosen graphene sheets. Moreover, the carbon nitride gases that are produced could provide carbon sources to form CNTs with the help of a cobalt catalyst. By the virtue of the simple pyrolysis process, a mass of pores could be simultaneously created, resulting in an open structural and porous material.

To investigate the morphology of as-prepared GN-CNT hybrids, scanning electron microscopy (SEM) images are presented in Figure 1. As seen, the GN-CNT hybrids clearly

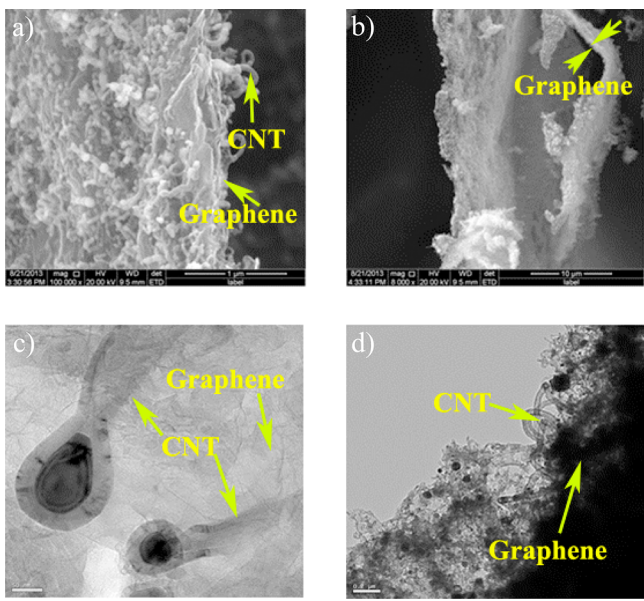


**Figure 1.** (a, b) SEM images of GN-CNT<sub>6.0</sub> and (c, d) TEM images of GN-CNT<sub>6.0</sub>.

show interlinked CNTs on the graphene flakes, where the well-defined CNTs have a diameter range of 25–35 nm and a length range of 163–525 nm (Figure 1a). From the side view, we found that CNTs were grown on both sides of graphene with a dense and uniform distribution (Figure 1b). It implies that such a method could successfully realize the growth of CNTs on GN via an effective adsorption of cobalt catalysts into the graphene layers. For control experiments, GN, GN-Co, and GN-urea samples were also prepared with the same procedure; their morphologies are compared in Figure S1 in the Supporting Information. It can be seen that both GN and GN-urea exhibit clean surfaces, without any appearance of nanotubes (see Figures S1a and S1b in the Supporting Information). Besides, GN-urea shows many more pores than GN, verifying that urea help to create a porous structure. Similarly, no CNTs were observed for GN-Co sample, while only disordered particles were found (Figure S1c in the Supporting Information). The results strongly demonstrate that GO, urea, and cobalt salt are essentially necessary for producing the expected 3D structured

GN-CNT hybrids. Furthermore, to examine the mechanical stability of CNTs on GN, as well as to verify that CNTs were chemically bonded to GN, not just physically adsorbed on GN, we ultrasonicated the GN-CNT for 30 min. We found that the CNTs adhered well to GN after ultrasonication, implying that CNTs were firmly linked with GN. Such a stable linkage of two different graphitic components was further investigated with TEM images. As shown in Figure 1c, the obtained CNTs are mainly multiwalled CNTs with an inner diameter of 16 nm and an outer diameter of ~32 nm. In addition, the cobalt-based catalysts were also identified as particles with the diameter of 36–122 nm, holding at the surface of GN and at the top of the CNTs. It suggests a tip growth mechanism of CNTs on GN, which agrees well with previously reported work.<sup>24,25</sup> A side view is also presented in Figure 1d, showing that the random growth of CNTs on GN by a stable linkage. However, note that the diameter of the CNTs ranged from 28 nm to 140 nm, which might be caused by different sizes of the adsorbed cobalt-based catalyst particles on GN. Nevertheless, with a facile pyrolysis method, we realized the growth of CNTs on both sides of GN. The well-characterized 3D structure of the hybrid is expected to exhibit good electron conductivity, low diffusion resistance of protons/cations, benign accessibility for the electrolyte, and high electroactive areas as electrode materials for high-performance SCs.

We further used X-ray diffraction (XRD) to characterize GN and GN-CNT to identify the chemical compositions of the samples, as shown in Figure 2a. A small amount of cobalt was observed with the GN-CNT sample, compared to the GN sample, which was indicated by the presence of typical peaks at 44.2° and 51.5°, corresponding to metallic cobalt. It is suggested that the metallic cobalt was formed during the growth of CNT, where the cobalt salt was reduced to metallic cobalt, as well as acting as a catalyst. Raman spectra of GN and GN-CNT samples are also shown in Figure 2b. The intensity ratio ( $I_D/I_G$ ) of D band and G band of GN is ~1.03, whereas the  $I_D/I_G$  value for GN-CNT is 1.51, implying that the graphitic crystalline structure of the GN is much better than that of GN-CNT. In other words, it means that the GN-CNT possesses a much more highly disordered graphitic structure, compared to GN, after the introduction of CNTs.<sup>26</sup> Furthermore, previous works have reported that the shape of the 2D band is strongly dependent on the number of graphene layers, where the 2D band becomes broader and asymmetric when the thickness increases.<sup>27</sup> As shown in the inset, the 2D band of GN-CNT is clearly sharper than that of GN, strongly demonstrating that GN-CNT has much fewer graphene layers than GN. Thus,

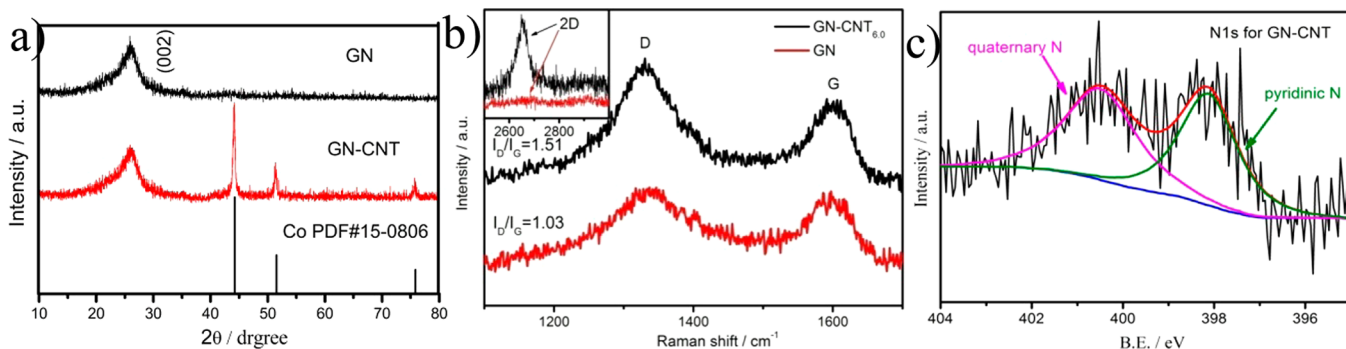


**Figure 2.** (a) XRD patterns of GN and GN-CNT<sub>6.0</sub>. (b) Raman spectra of GN-CNT<sub>6.0</sub> and GN; the inset shows an expanded view in the region of 2500–3000 cm<sup>-1</sup>. (c) High-resolution N 1s XPS spectra of GN-CNT<sub>6.0</sub>.

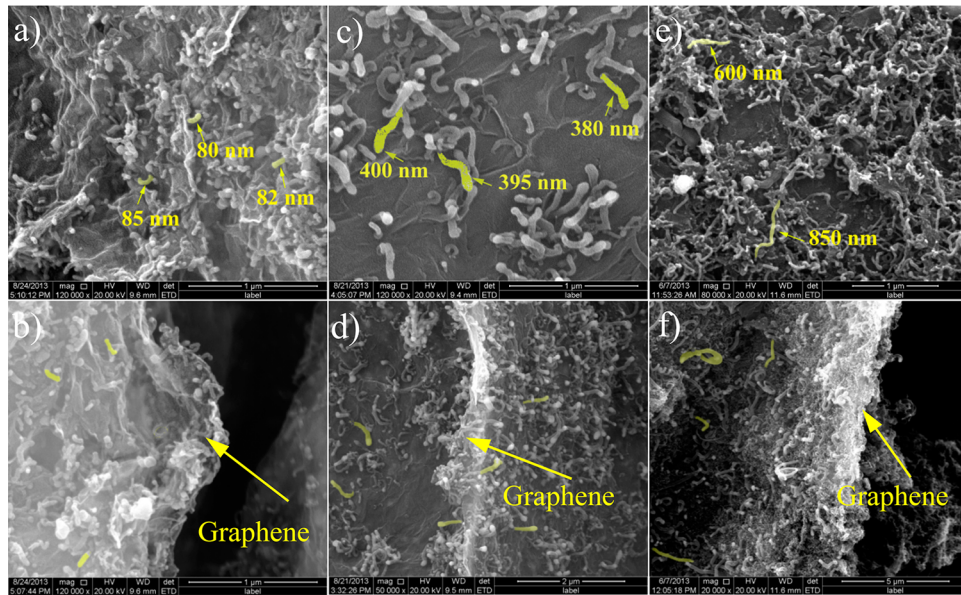


**Figure 3.** SEM images of (a, b) GN-CNT<sub>6.0</sub>, (c, d) GN-CNT<sub>15.0</sub>, and (e, f) GN-CNT<sub>30.0</sub>.

Raman results apparently prove that such a one-pot pyrolysis strategy could easily induce *in situ* growth of CNTs in the space of GN layers, resulting further interlayer expansion and structural distortion of GN. X-ray photoemission spectroscopy (XPS) spectrum of GN-CNT is presented, as shown in Figure 2c. The N 1s spectrum of GN-CNT shows pronounced peaks at 400.5 and 398.1 eV, corresponding to quaternary N and pyridinic N, respectively.<sup>28</sup> It suggests that the pyrolysis of urea could effectively nitridize the C atoms of the hybrid. The Brunauer–Emmett–Teller (BET) surface area was also tested to measure the specific surface area (see Figure S2 in the Supporting Information). It is believed that the introduction of CNTs into GN not only modifies the morphology, but also induces a large increase in specific surface area. The specific surface area of GN-CNT<sub>6.0</sub> was measured as 903 m<sup>2</sup> g<sup>-1</sup>, which is nearly 4.5-fold greater than that of graphene (205 m<sup>2</sup> g<sup>-1</sup>). Such a huge increase can be either ascribed to the effective intercalation and distribution of CNTs between graphene,<sup>13</sup> or could be due to the generation of a mass of pores during the release of a large amount of gases.<sup>9</sup> Furthermore, to identify the content of Co in GN-CNT<sub>6.0</sub>, thermogravimetric analysis was performed, as shown in Figure S3 in the Supporting Information. The ~400 °C decrease in temperature was attributed to the oxidation of cobalt species. Accordingly, the carbon/cobalt mass ratio in GN-CNT<sub>6.0</sub> is calculated to be 8:1.

Apart from the successful growth of CNTs on GN, we found that the length of the CNTs could be easily tuned by altering the amount of added urea in the precursor mixture. As such, it is reasonable to expect that the structure of the hybrid could be tailored and the performance could be optimized accordingly. To verify this, three samples of GN-CNT<sub>6.0</sub>, GN-CNT<sub>15.0</sub>, and GN-CNT<sub>30.0</sub> were prepared and the SEM images of the samples are presented. As shown in Figure 3a–f, it is clear that the length of the CNTs grown on GNs increases as the amount of urea in the precursor mixture increases. For the sample of GN-CNT<sub>6.0</sub>, CNTs have an average length of 80 nm. For the sample of GN-CNT<sub>15.0</sub>, the average length of CNTs increases to 400 nm, in addition to a higher density coverage at the GN surface. For the sample of GN-CNT<sub>30.0</sub>, it is obviously that the CNTs have a length range of 600–850 nm, which most of the

surface of the GN sample is clearly covered. Interestingly, we noted that when the additive amount of urea decreased to 3.0 g (GN-Co-urea<sub>3.0</sub>), no CNTs but only some particles were obtained, as shown in Figure S1d in the Supporting Information. This could be possibly explained by the fact that there are not enough carbon sources for the growth of CNTs with a low amount of urea. As such, we suggest that the percentage of urea in the mixture could not only control the length of the CNTs, but also adjust the surface coverage of CNTs on GN. Again, it demonstrates that urea plays a very important role in producing CNTs in the resultant nanocomposite.

With the unique structure, the GN-CNT is expected to show promising performance for the fabrication of SCs, because of its possible good electron conductivity, low diffusion resistance of protons/cations, ease of electrolyte penetration, and highly electroactive areas. Graphene has been reported as electrodes for SCs with a specific capacitance of 135 F g<sup>-1</sup> in aqueous KOH and 117 F g<sup>-1</sup> in H<sub>2</sub>SO<sub>4</sub> electrolyte.<sup>29,30</sup> Other types of GN-CNT hybrids have also been obtained and used for SCs.<sup>31</sup> However, the GN-CNT obtained with a one-pot pyrolysis strategy in this work is supposed to possess better performance, because of its remarkable physical properties. The electrochemical performance of as-prepared GN-CNT was first investigated by cyclic voltammetry (CV) in a three-electrode electrochemical cell. As shown in Figure 4a, GN-CNT<sub>6.0</sub> exhibits the CV curves of nearly rectangular shape, even at a scan rate of 1 V s<sup>-1</sup>, indicating ideal capacitive behavior, which is probably due to the high conductivity and fast ion transport of the GN-CNT<sub>6.0</sub> sample. We noted that, in contrast to the previously reported sandwiched CGS sample, only small redox peaks were found with GN-CNT, even though the cobalt catalyst was presented as demonstrated by XRD. This observation could be explained by the fact that only a very small amount of cobalt was utilized in our case, compared to that of sandwiched CGS.<sup>18</sup> According to the CV analyses, the specific capacitance of GN-CNT<sub>6.0</sub> was calculated to be 413 F g<sup>-1</sup> at a scan rate of 5 mV s<sup>-1</sup> in 6 M KOH solution, which is prominently higher than that of sandwiched CGS prepared via the combination of microwave treatment and traditional

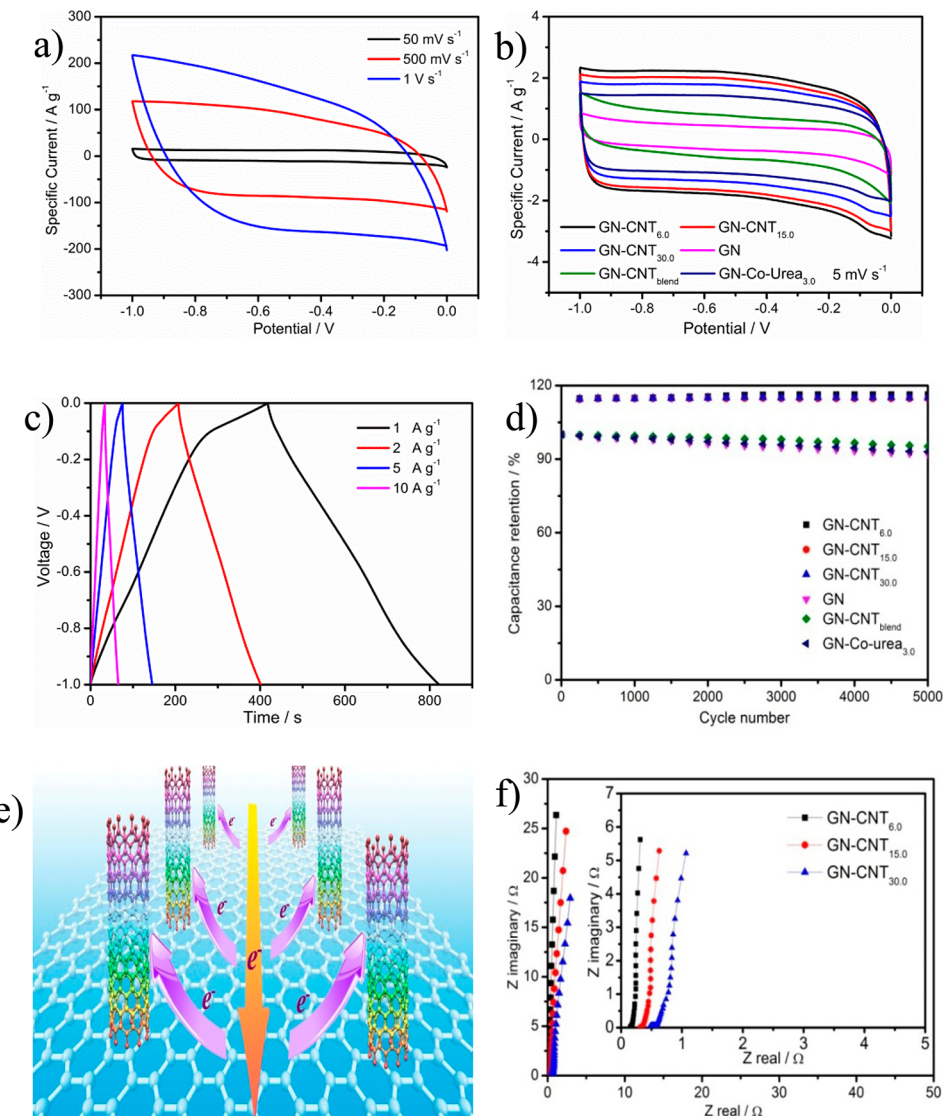


**Figure 4.** (a) Cyclic voltammograms of GN-CNT<sub>6.0</sub> in 6 M KOH solution with different scan rates. (b) Cyclic voltammograms of GN-CNT hybrids, GN, GN-CNT<sub>blend</sub>, and GN-Co-urea<sub>3.0</sub> in 6 M KOH solution at 5 mV s<sup>-1</sup>. (c) Galvanostatic charge/discharge curves for GN-CNT<sub>6.0</sub> at various discharge current densities. (d) Average specific capacitance versus cycle number for GN-CNT hybrids, GN-CNT<sub>blend</sub>, and GN at a galvanostatic charge and discharge current density of 1 A g<sup>-1</sup>. (e) Electron transfer path on GN-CNT hybrids. (f) Complex plane plot of the impedance; inset shows an expanded view in the region of high frequencies for GN-CNT hybrids.

CVD.<sup>18</sup> Such a promising performance of the hybrid might be contributed from both electrical double-layer capacitance (EDLC) of carbon composition and pseudo-capacitance possibly caused by the cobalt species. Furthermore, the CV curves of GN-CNT<sub>30.0</sub>, GN-CNT<sub>15.0</sub>, GN, GN-CNT<sub>blend</sub>, and GN-Co-urea<sub>3.0</sub> at the scan rate of 5 mV are shown in Figure 4b, in which the redox peak observed at approximately -0.1 V can be contributed to the cobalt species.<sup>32</sup> The specific capacitances are 394 F g<sup>-1</sup> for GN-CNT<sub>15.0</sub> and 387 F g<sup>-1</sup> for GN-CNT<sub>30.0</sub>, respectively. In contrast, GN-Co-urea<sub>3.0</sub>, GN-CNT<sub>blend</sub>, and GN only show low capacitances, of 268, 136, and 63 F g<sup>-1</sup>, respectively. As a result, the additive amount of 6.0 g of urea could achieve the highest specific capacitance. In comparison, although no CNTs were obtained and, thus, no unique GN-CNT structure was formed, GN-Co-urea<sub>3.0</sub> shows improved performance than GN and GN-CNT<sub>blend</sub>. This should be easily understood by its unique porous structure created by the pyrolysis of urea. When it comes to GN-CNT hybrids, we found that the presence of shorter CNTs on GN caused them

to be prone to exhibit higher capacitive behavior, which is in accordance with previous reports.<sup>33</sup> We next performed galvanostatic charge/discharge (CD) of GN-CNT<sub>6.0</sub> in a potential window from -1.0 V to 0 V at different current densities, as shown in Figure 4c. At current densities from 1 A g<sup>-1</sup> to 10 A g<sup>-1</sup>, the discharge curves of GN-CNT<sub>6.0</sub> are approximate straight lines, indicating ideal EDLC behavior of the electrode. The capacitance performances corresponding to different discharge current densities for the samples are presented in Figure S4a in the Supporting Information. A specific capacitance of 401 F g<sup>-1</sup> was achieved for GN-CNT<sub>6.0</sub> at a current density of 1 A g<sup>-1</sup>. Even at a high current density of 10 A g<sup>-1</sup>, a promising high capacitance of 271 F g<sup>-1</sup> for GN-CNT<sub>6.0</sub> is maintained. Such performance is apparently superior to that of GN. As a control experiment, the performance of GN-CNT<sub>blend</sub> was also measured, and the mechanical mixture obviously shows very poor SC performance, compared to GN-CNT. We further investigated the durability of the samples by carrying out continuous cycles tests. As shown in Figure 4d, a

capacitance increase of ca. 15% of the initial capacitance for GN-CNT<sub>6.0</sub> is observed after 5000 cycle tests, exhibiting excellent electrochemical stability of the sample. Such a 15% increase of the initial capacitance should be caused by activation of the cobalt species. Along with the operation in 6 M KOH in the applied potential range, the cobalt in GN-CNT hybrid should be oxidized to cobalt oxide. Cobalt oxide has been widely reported as a pseudo-capacitance material with high specific capacitance. Thus, it is reasonable to observe an increase in capacitance, along with the increased cycle number. A similar phenomenon has been observed in a previous study.<sup>18</sup> In contrast, the capacity retention for GN-Co-urea<sub>3.0</sub>, GN-CNT<sub>blend</sub>, and GN are 95%, 93%, and 92%, respectively. Based on the CV analyses, CD results, and durability tests, we conclude that all GN-CNT samples obtained with the proposed synthesis method possess better SC performance than GN and GN-CNT<sub>blend</sub>. In addition, we have noted that GN-CNT<sub>6.0</sub> shows the best performance among all the GN-CNT samples. We attribute the significant improvement of the SC performance of GN-CNT to the following possible reasons:

(1) The unique physical properties of GN-CNT hybrids, in terms of special interior structures, and large specific surface area are responsible for the high SC performance. As demonstrated above, the GN-CNT hybrid may benefit from the intercalation and distribution of CNTs between graphene layers. In contrast, pure GN suffers from the restacking during the annealing process, thus decreasing its specific surface area. The undesired restacking of GN leads to a great loss of electrical double-layer and poor capacitances, which is unavoidable in annealing-assist reduction of GO.<sup>34</sup> On the other hand, because of that condition, an open porous structure is highly favorable for high SC performance. Therefore, a mass of pores generated during the pyrolysis for GN-CNT hybrids helps to achieve high EDLC when applied in a voltage range.

(2) The synergistic effect between GN and CNTs in GN-CNT hybrids is another reason for the high capacitance performance. It is supposed that a unique 3D interconnected structure of GN-CNT hybrids, coupled with strong bonding between GN and CNTs, ensures ideal contact between GN and CNTs. Since both GN and CNTs possess intrinsic high electrical conductivity, the direct connection between the two components could contribute to fast electronic conductivity, thereby promoting energy storage (see Figure 4e). In contrast, it lacks good contact between GN and CNTs for the GN-CNT<sub>blend</sub> sample, thus leading to poor electrochemical behavior and low SC performance.

(3) XRD and TGA analysis have demonstrated the existence of cobalt species in GN-CNT hybrids. It is well-known that the cobalt species can deliver outstanding pseudo-capacitance. Thus, a pseudo-capacitance that is contributed from cobalt oxides contained in the GN-CNT hybrid helps to increase the overall performance.

(4) XPS analysis also shows that the pyrolysis of urea in this novel strategy can successfully nitrodize carbon materials. Such a nitrogen doping has been reported to promote the SC performance of carbon materials.<sup>35</sup> Therefore, the introduction of nitrogen into GN-CNT hybrid can induce high capacitance.

To identify such an assumption, the electrochemical property was further investigated by electrochemical impedance spectroscopy (EIS). Figure 4f displays the Nyquist plots of GN-CNT hybrids. The Nyquist plots of GN-CNT hybrids all show typical features of EDLC with a straight line, indicating an ideal capacitive behavior in the low-frequency region. Among the

three samples, GN-CNT<sub>6.0</sub> show the most vertical line, indicating the best SC behavior. This is because the small distance in short CNTs could minimize the electrolyte resistance by shortening the mean ionic diffusion pathway between the electrodes.<sup>25</sup> In contrast, all the samples of GN-Co-urea<sub>3.0</sub>, GN-CNT<sub>blend</sub>, and GN show a sloping trend (see Figures S4b–d in the Supporting Information). The value of the equivalent series resistance (ESR) includes the electrolyte resistance, the internal electrode resistance, and the electrical resistance between the electrode and the current collector, which can be obtained from the real axis intercept of the Nyquist plots. Since the electrolyte resistance and contact resistance between the electrode and the current collector are identical for all electrodes, ESR values can reflect the internal electrode resistance. The detected ESR values are 0.15, 0.31, and 0.47 Ω for GN-CNT<sub>6.0</sub>, GN-CNT<sub>15.0</sub>, and GN-CNT<sub>30.0</sub>, respectively. It was found that the ESR values increase as the amount of urea increases. This could be caused by the increase of the CNT length in the samples, which agrees well with the previously reported results.<sup>25</sup> From Figures S3b–d in the Supporting Information, the ESR value is obtained to be 0.58 for GN-Co-urea<sub>3.0</sub>, 0.62 for GN-CNT<sub>blend</sub>, and 0.80 for GN, respectively. Such a difference clearly demonstrated the synergistic effect between CNTs and GN in the as-prepared GN-CNT samples. As such, we believe that the 3D interconnected structure generated from our one-pot pyrolysis strategy could greatly reduce the ESR value and is favorable for energy conversion in SC applications.

We finally make a summary of the SC performances with a variety of carbon-material-based electrodes. As shown in Table S1 in the Supporting Information, among all the electrode materials prepared with different methods, the GN-CNT hybrid fabricated in this work shows the highest specific capacitance, as well as a promising durability (an increase of 15%, even after 5000 cycles). It strongly demonstrates that the one-pot pyrolysis strategy proposed in this work is an effective way to prepare a characteristic 3D GN-CNT composite as electrode material with fascinating SC performance.

## CONCLUSION

In summary, we have developed a one-pot pyrolysis strategy to prepare three-dimensional (3D) nanostructured GN-CNT hybrids as appealing supercapacitor (SC) electrode materials, which is substantially different from the previously reported methods in its cost-effective and facile manner. Apart from the well-defined 3D structure, the obtained GN-CNT hybrids exhibit controllable growth of CNTs on GN in their tunable length. Importantly, the unique structure of the hybrid endows it with remarkable physical properties, resulting in excellent electrochemical performances. The SC based on the as-prepared GN-CNT hybrid with a promising surface area of 903 m<sup>2</sup> g<sup>-1</sup> gives a high specific capacitance of 413 F g<sup>-1</sup>, as well as significant durability (115% after 5000 cycles). Therefore, we essentially pave a viable pathway to prepare 3D structured GN-CNT hybrids as high-performance SC electrode material. The method could also be easily expanded to prepare other carbon-oxide- or metal-oxide-based nanostructured composites for sensing, catalysis, and energy storage or conversion applications.

## ASSOCIATED CONTENT

### Supporting Information

SEM images of GN, GN-urea, GN-Co and GN-Co-urea<sub>3.0</sub>; N<sub>2</sub> adsorption–desorption isotherms for GN-CNT<sub>6.0</sub> and GN; specific capacitance of GN-CNT hybrids, GN-Co-urea<sub>3.0</sub>, GN, and GN-CNT<sub>blend</sub> at different discharge currents; complex plane plot of the impedance for GN-Co-urea<sub>3.0</sub>, GN-CNT<sub>blend</sub>, and GN; and comparison of the specific capacitance and cycling stability of some reported carbon-based SCs prepared with different strategies. This material is available free of charge via the Internet at <http://pubs.acs.org>.

## AUTHOR INFORMATION

### Corresponding Authors

\*E-mail: yanym@bit.edu.cn (Y.-M. Yan).

\*E-mail: bitkeneingsun@163.com (K.-N. Sun).

### Author Contributions

The manuscript was written through contributions of all authors. All authors have given approval to the final version of the manuscript.

### Notes

The authors declare no competing financial interest.

## ACKNOWLEDGMENTS

Financial support from the Ministry of Science and Technology (No. 2012DFR40240), National Natural Science Foundation of China (Grant No. 21175012), and the Chinese Ministry of Education (Project of New Century Excellent Talents in University) are gratefully acknowledged.

## REFERENCES

- (1) Novoselov, K. S.; Geim, A. K.; Morozov, S. V.; Jiang, D.; Zhang, Y.; Dubonos, S. V.; Grigorieva, I. V.; Firsov, A. A. Electric Field Effect in Atomically Thin Carbon Films. *Science* **2004**, *306*, 666–669.
- (2) Park, S.; Ruoff, R. S. Chemical Methods for the Production of Graphenes. *Nat. Nanotechnol.* **2009**, *4*, 217–224.
- (3) Yang, Z.-Y.; Jin, L.-J.; Lu, G.-Q.; Xiao, Q.-Q.; Zhang, Y.-X.; Jing, L.; Zhang, X.-X.; Yan, Y.-M.; Sun, K.-N. Sponge-Templated Preparation of High Surface Area Graphene with Ultrahigh Capacitive Deionization Performance. *Adv. Funct. Mater.* **2014**, DOI: 10.1002/adfm.201304091.
- (4) Meng, Y.; Zhao, Y.; Hu, C.; Cheng, H.; Hu, Y.; Zhang, Z.; Shi, G.; Qu, L. All-Graphene Core-Sheath Microfibers for All-Solid-State, Stretchable Fibriform Supercapacitors and Wearable Electronic Textiles. *Adv. Mater.* **2013**, *25*, 2326–2331.
- (5) Chen, P.; Xiao, T.-Y.; Qian, Y.-H.; Li, S.-S.; Yu, S.-H. A Nitrogen-Doped Graphene/Carbon Nanotube Nanocomposite with Synergistically Enhanced Electrochemical Activity. *Adv. Mater.* **2013**, *25*, 3192–3196.
- (6) Lee, D. H.; Kim, J. E.; Han, T. H.; Hwang, J. W.; Jeon, S.; Choi, S.-Y.; Hong, S. H.; Lee, W. J.; Ruoff, R. S.; Kim, S. O. Versatile Carbon Hybrid Films Composed of Vertical Carbon Nanotubes Grown on Mechanically Compliant Graphene Films. *Adv. Mater.* **2010**, *22*, 1247–1252.
- (7) Simon, P.; Gogotsi, Y. Capacitive Energy Storage in Nanostructured Carbon–Electrolyte Systems. *Acc. Chem. Res.* **2012**, *46*, 1094–1103.
- (8) Tsai, W. Y.; Lin, R. Y.; Murali, S.; Zhang, L. L.; McDonough, J. K.; Ruoff, R. S.; Taberna, P. L.; Gogotsi, Y.; Simon, P. Outstanding Performance of Activated Graphene Based Supercapacitors in Ionic Liquid Electrolyte from –50 to 80 Degrees C. *Nano Energy* **2013**, *2*, 403–411.
- (9) Daffos, B.; Taberna, P. L.; Gogotsi, Y.; Simon, P. Recent Advances in Understanding the Capacitive Storage in Microporous Carbons. *Fuel Cells* **2010**, *10*, 819–824.
- (10) Yang, Z.-Y.; Zhang, Y.-X.; Jing, L.; Zhao, Y.-F.; Yan, Y.-M.; Sun, K.-N. Beanpod-Shaped Fe-C-N Composite as Promising ORR Catalyst for Fuel Cells Operated in Neutral Media. *J. Mater. Chem. A* **2014**, *2*, 2623–2627.
- (11) Zhang, W.; Zhang, Y.; Tian, Y.; Yang, Z.; Xiao, Q.; Guo, X.; Jing, L.; Zhao, Y.; Yan, Y.; Feng, J.; Sun, K. Insight into the Capacitive Properties of Reduced Graphene Oxide. *ACS Appl. Mater. Interfaces* **2014**, *6*, 2248–2254.
- (12) Zhao, M.-Q.; Liu, X.-F.; Zhang, Q.; Tian, G.-L.; Huang, J.-Q.; Zhu, W.; Wei, F. Graphene/Single-Walled Carbon Nanotube Hybrids: One-Step Catalytic Growth and Applications for High-Rate Li-S Batteries. *ACS Nano* **2012**, *6*, 10759–10769.
- (13) Sun, T.; Zhang, Z.; Xiao, J.; Chen, C.; Xiao, F.; Wang, S.; Liu, Y. Facile and Green Synthesis of Palladium Nanoparticles-Graphene-Carbon Nanotube Material with High Catalytic Activity. *Sci. Rep.* **2013**, *3*, 2527.
- (14) Sharma, P.; Bhalla, V.; Dravid, V.; Shekhawat, G.; Jinsong, W.; Prasad, E. S.; Suri, C. R. Enhancing Electrochemical Detection on Graphene Oxide-CNT Nanostructured Electrodes Using Magneto-Nanobioprobes. *Sci. Rep.* **2012**, *2*, 877.
- (15) Varshney, V.; Patnaik, S. S.; Roy, A. K.; Froudakis, G.; Farmer, B. L. Modeling of Thermal Transport in Pillared-Graphene Architectures. *ACS Nano* **2010**, *4*, 1153–1161.
- (16) Dimitrakakis, G. K.; Tylianakis, E.; Froudakis, G. E. Pillared Graphene: A New 3-D Network Nanostructure for Enhanced Hydrogen Storage. *Nano Lett.* **2008**, *8*, 3166–3170.
- (17) Du, F.; Yu, D.; Dai, L.; Ganguli, S.; Varshney, V.; Roy, A. K. Preparation of Tunable 3D Pillared Carbon Nanotube-Graphene Networks for High-Performance Capacitance. *Chem. Mater.* **2011**, *23*, 4810–4816.
- (18) Fan, Z.; Yan, J.; Zhi, L.; Zhang, Q.; Wei, T.; Feng, J.; Zhang, M.; Qian, W.; Wei, F. A Three-Dimensional Carbon Nanotube/Graphene Sandwich and Its Application as Electrode in Supercapacitors. *Adv. Mater.* **2010**, *22*, 3723–3728.
- (19) Beidaghi, M.; Wang, C. Micro-Supercapacitors Based on Interdigital Electrodes of Reduced Graphene Oxide and Carbon Nanotube Composites with Ultrahigh Power Handling Performance. *Adv. Funct. Mater.* **2012**, *22*, 4501–4510.
- (20) Yu, D.; Dai, L. Self-Assembled Graphene/Carbon Nanotube Hybrid Films for Supercapacitors. *J. Phys. Chem. Lett.* **2010**, *1*, 467–470.
- (21) Chen, J.; Li, C.; Shi, G. Graphene Materials for Electrochemical Capacitors. *J. Phys. Chem. Lett.* **2013**, *4*, 1244–1253.
- (22) Hummers, W. S.; Offeman, R. E. Preparation of Graphitic Oxide. *J. Am. Chem. Soc.* **1958**, *80*, 1339–1339.
- (23) Lin, Z.; Waller, G.; Liu, Y.; Liu, M.; Wong, C.-P. Facile Synthesis of Nitrogen-Doped Graphene via Pyrolysis of Graphene Oxide and Urea, and its Electrocatalytic Activity toward the Oxygen-Reduction Reaction. *Adv. Energy Mater.* **2012**, *2*, 884–888.
- (24) See, C. H.; Harris, A. T. A Review of Carbon Nanotube Synthesis via Fluidized-Bed Chemical Vapor Deposition. *Ind. Eng. Chem. Res.* **2007**, *46*, 997–1012.
- (25) Otsuka, K.; Abe, Y.; Kanai, N.; Kobayashi, Y.; Takenaka, S.; Tanabe, E. Synthesis of Carbon Nanotubes on Ni/carbon-Fiber Catalysts under Mild Conditions. *Carbon* **2004**, *42*, 727–736.
- (26) Chae, S. J.; Guenes, F.; Kim, K. K.; Kim, E. S.; Han, G. H.; Kim, S. M.; Shin, H.-J.; Yoon, S.-M.; Choi, J.-Y.; Park, M. H.; Yang, C. W.; Pribat, D.; Lee, Y. H. Synthesis of Large-Area Graphene Layers on Poly-Nickel Substrate by Chemical Vapor Deposition: Wrinkle Formation. *Adv. Mater.* **2009**, *21*, 2328–2333.
- (27) Sun, Z.; Yan, Z.; Yao, J.; Beitler, E.; Zhu, Y.; Tour, J. M. Growth of Graphene from Solid Carbon Sources. *Nature* **2010**, *468*, 549–552.
- (28) Byon, H. R.; Suntivich, J.; Shao-Horn, Y. Graphene-Based Non-Noble-Metal Catalysts for Oxygen Reduction Reaction in Acid. *Chem. Mater.* **2011**, *23*, 3421–3428.
- (29) Stoller, M. D.; Park, S.; Zhu, Y.; An, J.; Ruoff, R. S. Graphene-Based Ultracapacitors. *Nano Lett.* **2008**, *8*, 3498–3502.

- (30) Vivekchand, S. R. C.; Rout, C. S.; Subrahmanyam, K. S.; Govindaraj, A.; Rao, C. N. R. Graphene-Based Electrochemical Supercapacitors. *J. Chem. Sci.* **2008**, *120*, 9–13.
- (31) Kim, Y.-S.; Kumar, K.; Fisher, F. T.; Yang, E.-H. Out-of-plane Growth of CNTs on Graphene for Supercapacitor Applications. *Nanotechnology* **2012**, *23*, 015301.
- (32) Chen, S.; Zhu, J.; Wang, X. One-Step Synthesis of Graphene–Cobalt Hydroxide Nanocomposites and Their Electrochemical Properties. *J. Phys. Chem. C* **2010**, *114*, 11829–11834.
- (33) Basirico, L.; Lanzara, G. Moving towards High-Power, High-Frequency and Low-Resistance CNT Supercapacitors by Tuning the CNT Length, Axial Deformation and Contact Resistance. *Nanotechnology* **2012**, *23*, 305401.
- (34) Liu, F.; Li, M.; Feng, Q.; Tang, N.; Zhong, W.; Huang, W.; Du, Y. Catalyst-Free Synthesis of Reduced Graphene Oxide-Carbon Nanotube Hybrid Materials by Acetylene-Assisted Annealing Graphene Oxide. *Appl. Phys. Lett.* **2012**, *101*, 123107.
- (35) Wen, Z.; Wang, X.; Mao, S.; Bo, Z.; Kim, H.; Cui, S.; Lu, G.; Feng, X.; Chen, J. Crumpled Nitrogen-Doped Graphene Nanosheets with Ultrahigh Pore Volume for High-Performance Supercapacitor. *Adv. Mater.* **2012**, *24*, 5610–5616.